Automated Iterative Csp^3-C Bond Formation

Daniel J. Blair[1]*, Sriyankari Chitti[1], Melanie Trobe[1], David M. Kostyra[1], Hannah M. S. Haley[1], Richard L. Hansen[2], Steve G. Ballmer[2], Toby J. Woods[3], Wesley Wang[1], Vikram Mubayi[1], Michael J. Schmidt[1], Robert W. Pipal[1], Greg. F. Morehouse[1], Andrea M. E. Palazzolo Ray[1], Danielle L. Gray[3], Adrian L. Gill[2] & Martin D. Burke[1,4,5,6]*

[1]Roger Adams Laboratory, School of Chemical Sciences, University of Illinois at Urbana-Champaign; 600 S. Mathews Avenue, Urbana, IL 61801, USA. [2]Department of Chemistry, REVOLUTION Medicines, Inc.; Redwood City, CA, USA. [3]George L. Clark X-Ray Facility and 3M Materials Laboratory, University of Illinois at Urbana-Champaign; 505 South Mathews Avenue, Urbana, IL 61801, USA. [4]Carle Illinois College of Medicine; 807 South Wright Street, Urbana, IL 61820, USA. [5]Arnold and Mabel Beckman Institute, University of Illinois at Urbana-Champaign; 405 North Mathews Avenue, Urbana, IL 61801, USA. [6]Department of Biochemistry, University of Illinois at Urbana-Champaign; 600 S. Mathews Avenue, Urbana, IL 61801, USA.

*e-mail: danielb@illinois.edu; mdburke@illinois.edu

Automated stereospecific assembly of Csp^3–C bonds would disruptively expand access to functional organic small molecules[1]. Methyliminodiacetic acid (MIDA) boronates are effective building blocks for automated small molecule synthesis[2], but are incompatible with stereospecific Csp^3-Csp^2 and Csp^3-Csp^3 bond forming reactions[3-19]. Here we report that hyperconjugative and steric tuning yielded a new class of tetramethyl *N*-methyliminodiacetic acid (TIDA) boronates that are stable to these conditions. Charge density analysis[20-22] revealed redistribution of electron density increases covalency of the N–B bond and thereby attenuates its hydrolysis. Complementary steric shielding of carbonyl π-faces decreases reactivity toward nucleophilic reagents. Unique features of the iminodiacetic acid cage[2] essential for generalized automated synthesis are retained by TIDA boronates. This allowed Csp^3 boronate building blocks to be assembled using automated synthesis, including first natural product syntheses that employ automated stereospecific Csp^3-Csp^2 and Csp^3-Csp^3 bond formation. These findings will enable increasingly complex Csp^3-rich small molecules to be accessed via automated assembly.

Automated iterative assembly of chemical building blocks broadens access to innovation at the molecular scale[1]. Methods for reversibly attenuating the reactivity of functional group handles used to link such blocks are critical for these platforms. For unsaturated (Csp^2-rich) organic small molecules, such lego-like assembly in automated and/or manual fashion has been achieved by many different research groups worldwide using *N*-methyliminodiacetic acid (MIDA) boronates[2,23-25] which are compatible with anhydrous basic Csp^2 cross-coupling conditions (Fig. 1a). An important advantage of MIDA relative to other ligands that attenuate boronic acid reactivity (e.g. dan, aam, ethanolamine, fluoride)[26] is that MIDA boronates display a tunable affinity for silica gel which permits generalized automated purification[2]. This unique feature enabled assembly of 14 distinct classes of small organic molecules using one automated process[2].

Important areas of chemical space remain inaccessible with this first-generation platform, particularly for molecules rich in non-planar and potentially stereogenic sp^3-hybridized carbon atoms (Csp^3). This represents a significant limitation, because Csp^3-rich molecules constitute some of the most impactful natural products, medicines[27], biological probes, and functional materials[28]. An important goal is thus to expand automated modular synthesis to include Csp^3-rich small molecules.

Many recent breakthroughs in stereospecific formation of Csp^3-C bonds through Suzuki-Miyaura couplings[3-11] and 1,2-metallate reactions[12-19] stand to enable advances in this direction (Fig. 1b). However, most of these reactions either require aqueous basic conditions that hydrolyze MIDA boronates, or nucleophilic reagents that react with MIDA boronates (Fig. 1c). In both cases loss of the MIDA protecting group will lead to uncontrolled couplings and form complex mixtures and/or oligomeric products. We thus sought hyperstable boronates to enable lego-like small molecule synthesis *via* iterative Csp^3-C bond formation.

Identifying a hyperstable boronate

Mechanistic studies on MIDA boronate hydrolysis provided foundation for developing hyperstabilized variants[29]. There are two mechanisms for MIDA boronate hydrolysis. The first involves frustrated Lewis pair-like activation of water by the dative N–B bond. The second mechanism involves ester hydrolysis-like cleavage of a MIDA carbonyl (C=O) group by hydroxide. Steric shielding would likely protect the carbonyl carbons from hydroxide and nucleophiles, yet steric effects are known to activate frustrated Lewis pair behavior of N-B bonds[30-32]. And although hydrolysis studies of MIDA boronates[29] indicated electronic tuning of the N-B bond could be achieved

via modifying the organic group attached to boron, we required a building block independent solution. So, at the outset it was unclear whether steric or electronic effects could be leveraged to create a more stable ligand.
Using ^{18}O-water to probe the hydrolysis of MIDA boronate **1a**[29], we first established the N–B bond as the primary hydrolysis mechanism under aqueous basic Csp^3-Csp^2 Suzuki-Miyaura coupling conditions (THF/H_2O, K_2CO_3, 60 °C)(Fig. 2a). We thus required a MIDA derivative which could suppress the frustrated Lewis pair-like reactivity of the N–B bond. To better understand this behavior, we used ^1H NMR to study the stability of a range of substituted MIDA derivatives (**1b**, **3**-**9**) in deuterated solvent (THF-d_8/D_2O, K_2CO_3, 60 °C) (Fig. 2b).
Consistent with prior precedent[31,32], bulky groups on nitrogen (Fig. 2b **3**-**5** and Fig. S2a) increased the rate of hydrolysis relative to MIDA (**1b**), likely increasing N-B frustrated Lewis pair-like behavior. Remarkably, appending two *n*-butyl groups (**6**) to the iminodiacetic acid backbone caused almost no change in hydrolysis rate relative to MIDA (**1b**). Reducing the size of these substituents to ethyl groups (**7**) and methyl groups (**8**) provided more impressive stabilization. Finally, we prepared a boronate derived from a highly sterically hindered tetramethylated variant of *N*-methyliminodiacetic acid **9** (TIDA) and, surprisingly, found it was highly stable under aqueous basic Csp^3-Csp^2 cross coupling conditions, with >99% remaining after 6 h (Fig. 2b).
Additional hydrolysis studies of TIDA boronate **21** under these conditions in protic solvent (Fig S3, S4), ^{18}O labelling (Fig. S5), and neutral hydrolysis (Fig. S6) indicated that TIDA boronates were cleaved *via* N–B bond water activation. The hyperstable TIDA boronate was retained during Csp^3-Csp^2 Suzuki-Miyaura reaction between Csp^3-boronate **10** and bifunctional halo-TIDA boronate **11b** to provide **12**, whereas MIDA boronate **11a** (Fig. 2c) and related BIDA boronate **SI-14** (Fig. S2b) gave no desired product.
Encouraged by these results, we tested the stability of TIDA boronates to iPrMgCl.LiCl, which promotes Csp^3-Csp^3 bond forming 1,2-metallate reactions[18] (Fig. 2d). TIDA boronate **14b** resists cleavage by iPrMgCl.LiCl to form the target product **15** in high yield and stereospecificity, whereas MIDA boronate **14a** is cleaved under these conditions. Remarkably, TIDA boronates even tolerated highly reactive *t*BuLi, enabling the formation of **18** and **19** in excellent diastereoselectivity (Fig. 2e). Providing an additional practical advantage, our bifunctional sulfoxide[18]-TIDA boronate building blocks (i.e. **14**, **16** and **17**) are easily handled bench stable solids (Fig S1).

X-ray crystallographic studies

The stability of **9** toward aqueous base is surprising considering the strong precedent for *increased* reactivity of frustrated Lewis pairs derived from tetramethylpiperidine[30]. Hints at the origin of this stability were found upon x-ray crystallographic analysis of single crystals of MIDA boronate **1c** (Fig. 3a, *inset*) and TIDA boronate **20** (Fig. 3b, *inset*) which revealed a >10° torsional shift along the N-B axis in TIDA **20** relative to MIDA **1c**.
Torsional effects can substantially influence[33] the magnitude of hyperconjugative stabilization (i.e. staggered vs eclipsed ethane[34]). Torsional shifts in **20** bring three donor N-C bonds nearly antiperiplanar to three acceptor bonds (two B-O bonds and one B-C bond), potentially elevating hyperconjugation across the N-B bond. Backbone methylation would likely increase N-C donor ability, and internal angle compression in **20** (~5°) suggests thermodynamic Thorpe-Ingold effects rigidify the framework (Extended Data Fig. 1a). Both effects likely reinforce putative hyperconjugation across the N-B bond in **20**. We thus questioned whether stabilizing hyperconjugative interactions across the N-B bond in TIDA boronates drive a reduction in the rate of N-B hydrolysis.

Electron distribution analysis

To experimentally probe electronic effects, we performed Quantum Theory of Atoms in Molecules (QTAIM)-based charge density analysis[20-22] on x-ray crystal structures of MIDA boronate **1c** and TIDA boronate **20**. Multiple lines of evidence revealed that the dramatic reduction in hydrolysis for TIDA boronates is attributable to hyperconjugation-mediated redistribution of electron density that increases covalency of the N-B bond.
Topology maps of crystallography determined bonding electron density ρ demonstrated electron redistribution across planar slices spanning the iminodiacetic acid rings of MIDA **1c** and TIDA **20** (Fig. 3a,b). Notable features of TIDA **20** included increased electron density spanning the N-B interatomic space (Fig 3b, Extended Data Fig. 2j), and formation of a contiguous ring of electron density around the iminodiacetic acid cage (Fig. 3b). The stabilizing nature of electronic redistribution with the N-B bond of TIDA **20** was supported by a negative Laplacian $\nabla^2\rho(r)$ at boron and nitrogen valence shell charge concentrations (Extended Data Fig. 3j). TIDA **20** therefore possesses an N-B bond of substantially increased covalent character.
Elongation of nitrogen attached donor bonds and boron attached acceptor bonds (Extended Data Fig. 1b), consistent with prior studies of anomeric[35] and gauche effects[36], supports three-fold hyperconjugation along the

N-B linkage. Anticipated increased π-character manifested localized increased ellipticity (ε)[20] (Extended Data Fig. 4c,f,g,j,l,m), and redistributed electron density was supported by changes in $\nabla^2\rho(r)$ (Extended Data Fig. 3e,f,k[37]. Electrostatic potential maps, reduced polarization of the N-B bond[38], and $^{11}B/^{13}C$ NMR shifts were also consistent with electron redistribution (Extended Data Fig. 5). Additional stabilizing electronic redistributions were found upon examination of ρ, $\nabla^2\rho(r)$, and ε surrounding boron attached oxygens O1 and O4 which revealed more equal distribution of electron density directed toward boron and the carbonyl carbons for TIDA **20** compared to MIDA **1c** (Extended Data Fig. 2b,c,h,i, 3b,c,h,i, 4c,d,i,j and 6).

Increased electron sharing[39] is consistent with reduced propensity for frustrated Lewis pair activity[40-42], and rationalizes the increased robustness of TIDA boronates toward N–B bond hydrolysis. Remarkably, these stark differences in N–B bond character are contrasted with similar bond length [MIDA **1c**: 1.6613(7) Å; TIDA **20**: 1.6632(5) Å].

Steric shielding of TIDA boronates

Crystallographic data for TIDA **20** also indicated that the stability of TIDA boronates toward carbon nucleophiles (iPrMgCl.LiCl and tBuLi) arises from shielding of all four π-faces of the carbonyls by the attached methyl groups (Fig. 3c, Extended Data Fig. 7a[43]). Comparison to organolithium-stable Beak-type benzoates[44] revealed that **20** mirrors Beak-like shielding interactions *via* a trans-annular methyl group spanning the back face of the iminodiacetic acid cage (Extended Data Fig. 7b).

Synthetic utility of TIDA boronates

Reversible ligation is a requirement for deploying TIDA boronates in iterative cross coupling-based building block assembly. An orthogonal pathway for hydrolysis involving C=O attack (Fig S7, Extended Data Fig. 8a) enabled TIDA boronates (**21**) to be deprotected to boronic acids (**22**), trifluroborate salts (**23**), and boronic esters[45] (**24**, **25**) by simply using aqueous basic or protic conditions at elevated temperature (Fig. 3d).

TIDA boronates retain all other key features of their MIDA boronate counterparts that enabled automated building block-based synthesis[2]: TIDA ligand is accessible on kg-scale (Extended Data Fig. 8b), TIDA boronates are prepared from boronic acids under Dean-Stark conditions or by using a dehydrated form of TIDA (Extended Data Fig. 8c), TIDA boronates are stable to a wide range of common cross coupling reactions (i.e. Stille, Suzuki, Sonogashira, Heck, photochemical, see Extended Data Fig. 9), and chemical transformations (i.e. oxidation, reduction, borylation, olefination, see Extended Data Fig. 10). Representative TIDA boronates retain a tunable affinity for silica gel, being minimally mobilized in Et_2O and rapidly eluted in THF (Extended Data Fig. 8d). This feature enables the TIDA boronate group to act as a tag for generalized and automated catch-and-release purification[2]. The heightened stability of TIDA boronates further enabled us to create a self-contained next generation synthesis machine (Fig. S8-11, S13) to enable automated iterative assembly of Csp^3 boronate building blocks (Fig 4a,d).

Having established an iterative synthesis platform (Fig. 4a), we investigated a series of stereospecific Csp^3-Csp^2 cross-coupling reactions with bifunctional halo TIDA boronates (Fig. 4b). Across a range of carbonate promoted aqueous/protic stereospecific Csp^3 cross coupling reactions, MIDA boronates were fully hydrolyzed, whereas the corresponding TIDA boronates universally provided the desired products in good yields both in manual and automated formats (**12**, **26**, **27**, and **28**). The increased stability of TIDA boronates also permitted use of stronger bases KOH[9] (**31**) and Ag_2O[7] (**30**).

Leveraging automated Csp^3-Csp^2 couplings with TIDA boronates, we targeted a lego-like total synthesis of ieodomycin C[46] (Fig. 4c). Building block **31** (97:3 *er*) underwent automated stereospecific Csp^3 cross-coupling with bifunctional TIDA boronate **32** to provide **33** in >95:5 *er* and 50% isolated yield after automated purification. TIDA boronate enabled functional group interconversion followed by deprotection (**34**) and Suzuki-Miyaura cross coupling with vinyl halide **35** furnished diene **36**, and ieodomycin C after deprotection.

The tolerability of TIDA boronates to iPrMgCl.LiCl allowed 1,2-metallate reactions to be executed with bifunctional sulfoxide-TIDA boronate building blocks in manual and automated formats (Fig. 4d) to prepare a variety of Csp^3-Csp^3 bonds in excellent yields (Fig. 4e, **15** and **37-42**). A triply-boron selective reaction was also achieved in the diastereospecific preparation of **43** and **44**. Csp^2 boronic esters were also effective (**45**, **46**).

Reactivity differences between unhindered/hindered boronic esters[47,48] suggested potential for iteration-enabling kinetic selectivity within Csp^3-Csp^3 bond formation. Accordingly, we investigated the lego-like automated synthesis of macrocyclic antifungal natural product sch 725674[49] (Fig. 4f). Demonstrating the advantage of our

approach over prior strategies[50] to access sch725674, our bifunctional sulfoxide-TIDA boronate **14b** enabled recursive application of the same assembly chemistries to form Csp^3-Csp^3 bonds. Additionally, the inclusion of a TIDA boronate allowed this entire process of multiple building block assembly *via* iterative Csp^3-Csp^3 bond formation to be executed in a fully automated and uninterrupted fashion (Fig S14,15). *n*-Pentyl pinacol boronic ester **47** was subject to 1,2-metallate reaction with sulfoxide-boronate **14** to afford the target TIDA boronate **48** in high enantioselectivity (>95:5 *er*). Automated deprotection to the corresponding pinacol boronic ester **49** was followed by automated boronic ester-selective reaction with sulfoxide **50** to provide the core carbon scaffold of sch725674 (**52**) after oxidation. Deprotection (TBAF, **53**), oxidative modification, macro-lactonization, and final deprotection furnished sch725674 in only 7 steps from bench stable building blocks.

Conclusion

Many different types of stereospecific Csp^3-C bond forming methods can now be employed in manual and automated building block-based synthesis pathways. This advance was enabled by the discovery of TIDA boronates that tolerate both aqueous basic conditions and reactive carbon nucleophiles. This represents an important step towards the automated lego-like synthesis of Csp^3-rich organic small molecules and materials that perform a broad range of important functions.

References

1. Trobe, M. & Burke, M. D. The molecular industrial revolution: automated synthesis of small molecules. *Angew. Chem. Int. Ed.* **57**, 4192-4214, (2018).

2. Li, J., Ballmer, S. G., Gillis, E. P., Fukii, S., Schmidt, M. J., Palazzolo, A. M. E., Lehmann, J. W., Morehouse, G. F. & Burke, M. D. Synthesis of many different types of organic small molecules using one automated process. Science **347**, 1221-1226, (2015).

3. Imao, D., Glasspoole, B. W., Laberge, V. S. & Crudden, C. M. Cross coupling reactions of chiral secondary organoboronic esters with retention of configuration. *J. Am. Chem. Soc.* **131**, 5024-5025, (2009).

4. Lee, J. C. H., McDonald, R. & Hall, D. G. Enantioselective preparation and chemoselective cross-coupling of 1,1-diboron compounds. *Nat. Chem.* **3**, 894-899, (2011).

5. Awano, T., Ohmura T. & Suginome, M. Inversion or Retention? Effects of acidic additives on the stereochemical course in enantiospecific Suzuki-Miyaura coupling of α-(acetylamino)benzylboronic esters. *J. Am. Chem. Soc*. **133**, 20738-20741, (2011).

6. Li, L., Zhao, Z., Joshi-Pangu, A., Diane, M. & Biscoe, M. R. Stereospecific Pd-catalyzed cross-coupling reactions of secondary alkylboron nucleophiles and aryl chlorides. *J. Am. Chem. Soc.* **136**, 14027-14030, (2014).

7. Lehmann, J. W., Crouch, I. T., Blair, D. J., Trobe, M., Wang, P., Li, J. & Burke, M. D. Axial shielding of Pd(II) complexes enables perfect stereoretention in Suzuki-Miyaura cross-coupling of Csp^3 boronic acids. *Nature Communications* **10**, 1263, (2019).

8. Sandrock, D. L., Jean-Gerard, L., Chen, C.-Y., Dreher, S. D. & Molander, G. A. Stereospecific cross-coupling of secondary alkyl β-trifluoroboratoamides. *J. Am. Chem. Soc*. **132**, 17108-17110, (2010).

9. Mlynarski, S. N., Schuster, C. H. & Morken, J. P. Asymmetric synthesis from terminal alkenes by cascades of diboration and cross-coupling. *Nature* **505**, 386-390, (2013).

10. Blaisdell, T. P., & Morken, J. P. Hydroxyl-directed cross-coupling: a scalable synthesis of debromohamigeran E and other targets of interest. *J. Am. Chem. Soc.* **137**, 8712-8715, (2015).

11. Zhao, S., Gensch, T., Murray, B., Niemeyer, Z. L., Sigman, M. S. & Biscoe, M. R. Enantiodivergent Pd-catalyzed C–C bond formation enabled through ligand parameterization. *Science* **362**, 670-674, (2018).

12. Leonori, D. & Aggarwal, V. K. Lithiation-borylation methodology and its application in synthesis. *Acc. Chem. Res. **47***, 3174-3183, (2014).

13. Sharma, H. A., Essman, J. Z. & Jacobsen, E. N. Enantioselective catalytic 1,2-boronate rearrangements *Science **374***, 752-757, (2021).

14. Zhang, L., Lovinger, G. J., Edelstein, E. K., Szymaniak, A. A., Chierchia, M. P. & Morken, J. P. Catalytic conjunctive cross-coupling enabled by metal-induced metallate rearrangement. *Science **351***, 70-74, (2016).

15. Schmidt, J., Choi, J., Liu, A. T., Slusarczyk, M. & Fu, G. C. A general, modular method for the catalytic asymmetric synthesis of alkylboronate esters. *Science **345***, 1265-1269, (2016).

16. Linne, Y., Bonandi, E., Tabet, C., Geldsetzer, J. & Kalesse, M. The total synthesis of chondrochloren A. *Angew. Chem. Int. Ed. **60***, 6938-6942 (2021).

17. Burns, M., Essafi, S., Bame, J. R., Bull, S. P., Webster, M. P., Balieu, S., Dale, J. W., Butts, C. P., Harvey, J. N. & Aggarwal, V. K. Assembly-line synthesis of organic molecules with tailored shapes. *Nature* ***513***, 183-188, (2014).
18. Casoni, G., Kucukdisli, M., Fordham, J. M., Burns, M., Myers, E. L. & Aggarwal, V. K. α-Sulfinyl benzoates as precursors to Li and Mg carbenoids for the stereoselective iterative homologation of boronic esters. *J. Am. Chem. Soc.* ***139***, 11877-11886, (2017).
19. Matteson, D. S. Boronic esters in asymmetric synthesis. *J. Org. Chem.* ***78***, 10009-10023, (2013).
20. Bader, R. F. W., Slee, T. S., Cremer, D. & Kraka, E. Description of conjugation and hyperconjugation in terms of electronic distributions. *J. Am. Chem. Soc.* **105**, 5061-5068, (1983).
21. Bader, R. F. W. Ed., *Atoms in Molecules-A Quantum Theory* (Oxford University Press, Oxford, 1990).
22. Koritsanszky, T. S. & Coppens, P. Chemical applications of x-ray charge-density analysis. *Chem. Rev.* **101**, 1583-1628, (2001).
23. Fujita, K., Matsui, R., Suzuki,T. & Kobayashi, S. Concise Total Synthesis of (-)-Myxalamide A. *Angew. Chem. Int. Ed.* **51**, 7271-7274, (2012).
24. Seo, K.-B., Lee, I.-H., Lee, J., Choi, I. & Choi, T.-L. A rational design of highly controlled Suzuki-Miyaura catalyst-transfer polycondensation for precision sysnthesis of polythiophenes and their block copolymers: marriage of palladacycle precatalysts with MIDA-boronates. *J. Am. Chem. Soc.* **140**, 4335-4343, (2018).
25. Angelone, D., Hammer, A. J. S., Rohrbach, S., Krambeck, S., Granda, J. M., Wolf, J., Zalesskiy, S., Chisholm, G. & Cronin, L. Convergence of multiple synthetic paradigms in a universally programmable chemical synthesis machine. *Nature Chemistry* **13**, 63-69, (2021).
26. Lennox, A. J. J. & Lloyd-Jones, G. C. Selection of boron reagents for Suzuki-Miyaura coupling. *Chem. Soc. Rev.* **43**, 412-443, (2014).
27. Lovering, F., Bikker, J., & Humblet, C. Escape from flatland: increasing saturation as an approach to improving clinical success. *J. Med. Chem.* **52**, 6752-6756, (2009).
28. Worch, J. C., Prydderch, H., Jimaja, S., Bexis, P., Becker, M. L., & Dove, A. P. Stereochemical enrichment of polymer properties. *Nat. Rev. Chem.* **3**, 514-535, (2019).
29. Gonzalaez, J. A., Maduka Ogba, O., Morehouse, G. F., Rosson, N., Houk, K. N., Leach, A. G., Cheong, P. H. Y., Burke, M. D., & Lloyd-Jones, G. C. MIDA boronates are hydrolysed fast and slow by two different mechanisms. *Nat. Chem.* **8**, 1067-1075, (2016).
30. Stephan, D. W. & Erker, G. Frustrated Lewis pairs: metal-free hydrogen activation and more. *Angew. Chem. Int. Ed.* **49**, 46-76, (2010).
31. Mancilla, T. & Contreras, R. New bicylic organylboronic esters derived from iminodiacetic acids. *J. Organomet. Chem.* **307**, 1-6, (1986).
32. Mancilla, T., de los Ángeles Calixto Romo, M. & Delgado, L. A. Synthesis and characterization of (N->B) phenyl[N-alkyl-N-(2-alkyl)aminodiacetate-O,O',N]boranes and phenyl[N-alkyl-N-(2-alkyl)aminodiacetate-O,O',N]boranes. *Polyhedron* **26**, 1023-1028, (2007).
33. Wu, J. I-C. & Ragué Schelyer, P. von, Hyperconjugation in hydrocarbons: Not just a "mild sort of conjugation" *Pure Appl. Chem.* ***85***, 921-940, (2013).
34. Pophristic, V. & Goodman, L. Hyperconjugation not steric repulsion leads to the staggered structure of ethane. *Nature* ***411***, 565-568, (2001).
35. Senderowitz, H., Golender, L. & Fuchs B. New supramolecular host systems. 2. 1,3,5,7-Tetraoxadecalin, 1,2-dimethoxyethane and the gauche effect reappraised. Theory vs. experiment. *Tetrahedron* ***32***, 9707-9728, (1994).
36. Hoffman, R. W., Hrovat, D. A. & Borden, W. T. Is hyperconjugation responsible for the "gauche effect' in 1-fluoropropane and other 2-subsituted-1-fluoroethanes? *J. Chem. Soc. Perkin Trans 2*, 1719-1726, (1999).
37. Scherer, W., Sirsch, P., Shorokhov, D., McGrady, G. S., Mason, S. A. & Gardiner, M. G. Valence-shell charge concentrations and electron delocalization in alkyllithium complexes: negative hyperconjugation and agnostic bonding. *Chem. Eur. J.* ***8***, 2324-2334, (2002).
38. Hirschfeld, F. L. Bonded-atom fragments for describing molecular charge densities. *Theor. Chim. Acta.* **44**, 129-138, (1977).
39. Jonas, V., Frenking, G. & Reetz, M. T. Comparative theoretical study of Lewis acid-base complexes of BH_3, BF_4, BCl_3, $AlCl_3$, and SO_2. *J. Am. Chem. Soc.* **116**, 8741-8753, (1994).

40. Skara, G., de Vleeschouwer, F., Geerlings, P., de Proft, F. & Pinter, B. Heterolytic splitting of molecular hydrogen by frustrated and classical Lewis pairs: a unified reactivity concept. *Scientific Reports* **7**, 16024, (2017).
41. Schürmann, C. J., Herbst-Irmer, R., Teuteberg, T. L., Kratzert, D., Erker, G., Mata, R. A. & Stalke, D. Experimental charge density study on FLPs and a FLP reaction product. *Z. Kristallogr. – Crystalline Materials* **233**, 723-731, (2018).
42. Ullrich, M., Lough, A. J. & Stephan D. W., Dihydrogen activation by $B(p\text{-}C_6F_4H)_3$ and phosphines, *Organometallics* **29**, 3647-3654, (2010).
43. Falivene, L., Cao, Z., Petta, A., Serra, L., Poater, A., Olivia, R., Scarano, V. & Cavallo, L. Towards the online computer-aided design of catalytic pockets *Nature Chemistry* ***11***, 872-879, (2019).
44. Beak, P. & Carter, L. G. Dipole-stabilized carbanions from esters: α-oxo lithithiations of 2,6-substituted benzoates of primary alcohols. *J. Org. Chem.* ***46***, 2363-2373, (1981).
45. Landry, M. L., Hu, D. X., McKenna, G. M. & Burns N. Z. Catalytic enantioselective dihalogenation and the selective synthesis of (-)-deschloromytilipin A and (-)-danicalipin A. *J. Am. Chem. Soc.* ***138***, 5150-5158, (2016).
46. Mojid Mondol, M. A., Kim, J. H., Lee, M. A., Tareq, F. S., Lee, H.-S., Lee, Y.-J. & Shin, H. J. Ieodomycins A-D, antimicrobial fatty acids from a marine Bacillus sp., *J. Nat. Prod.* **74**, 1606-1612, (2011).
47. Blakemore, P.R., Marsden, S. P. & Vater, H. D. Reagent-controlled asymmetric homologation of boronic esters by enantioenriched main-group chiral carbenoids. *Org. Lett.* ***8***, 773-776, (2006).
48. Roesner, S., Blair, D. J. & Aggarwal V. K. Enantioselective installation of adjacent tertiary benzylic stereocentres using lithiation-borylation-protodeboronation methodology. Application to the synthesis of bifluranol and fluorohexestrol. *Chem. Sci.* ***6***, 3718-3723, (2015).
49. Yang, S.-W., Chan, T.-M, Terracciano, J., Loebenberg, D., Patel, M. & Chu, M. Structure elucidation of sch725674 from Aspergillus sp. *J. Antibiot.* ***58***, 535-538, (2005).
50. Fawcett, A., Nitsch, D., Ali M., Bateman, J. M., Myers, E. L. & Aggarwal V. K. Regio- and stereoselective homologation of 1,2-bis(boronic esters): stereocontrolled synthesis of 1,3-diols and sch 725674. *Angew. Chem. Int. Ed.* ***55***, 14663-14667, (2016).
51. Momma, K. & Izumi F. VESTA 3 for three-dimensional visualization of crystal, volumetric and morphology data. *J. Appl. Crystallogr.* ***44***, 1272-1276, (2011).
Acknowledgments We thank Furong Sun and Haijun Yao at the UIUC Mass Spectrometry Facility, Dean Olson, Lingyang Zhu, and Nikki Duay at the School of Chemical Sciences NMR Lab at UIUC for NMR services, and members of the Burke laboratory for discussions related to this project. The Bruker 500 MHz NMR spectrometer was obtained with the financial support of the Roy J. Carver Charitable Trust, Muscatine, Iowa, USA. D.J.B. would like to thank the Damon-Runyon Cancer Research Foundation for their unwavering support during the COVID-19 pandemic. Scott Denmark is also gratefully acknowledged for thoughtful manuscript review. We thank Peng-Jui Chen, Yuquan Tong, Andrew Blake, Harpreet Auby, and Daniel Szczepankiewicz for technical assistance. Support was provided by the following sources: M.D.B - NIH (GM118185), NSF (CHE-1955838), D.J.B - Illini 4000 Fellow of the Damon-Runyon Cancer Research Foundation DRG-2290-17, S.C. - ACS Division of Organic Chemistry Summer Undergraduate Research Fellowship, Henry Luce Foundation and the Illinois Scholars Undergraduate Research Program, M.B.T. - Erwin Schrödinger Post-Doctoral Fellow, Austrian Science Fund (FWF):[J3960-N34].
Competing Interests The University of Illinois has filed patent applications related to MIDA and TIDA boronates. M.D.B is a Founder, shareholder, and consultant for REVOLUTION Medicines.
Author Contributions Project was designed by D.J.B., M.J.S., and M.D.B. Experimental work was conducted by D.J.B., S.C., M.B.T., D.M.K, H.M.S.H., R.L.H., S.G.B., T.W., W.W., V.M., M.J.S., R.W.P., G.F.M., A.M.E.P.R. and D.L.G. Automated synthesis experiments were performed by D.J.B., M.B.T. and H.M.S.H with guidance from R.L.H. and S.G.B. Crystallographic data were collected by T.W. and D.L.G. Multipole structural refinements were performed by T.W. Small molecule synthesis machines were designed, constructed, and finalized by R.L.H., S.G.B., A.L.G. and M.D.B. D.J.B and M.D.B. wrote the manuscript.
Supplementary Information is available for this paper at
Correspondence and requests for materials should be addressed to D.J.B. or M.D.B.
Reprints and permissions information is available at http://www.nature.com/reprints.

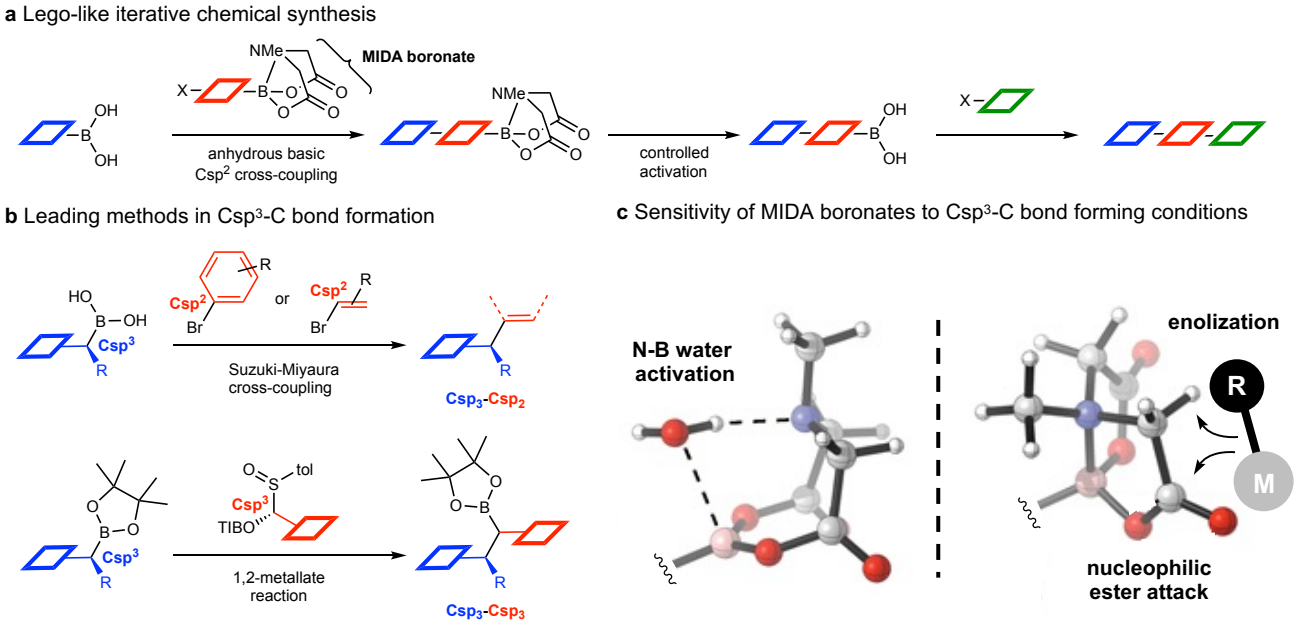

Fig. 1 | Lego-like chemical synthesis. a. Automated synthesis is achieved using bifunctional MIDA boronate building blocks. Controlled removal of MIDA enables iterative synthesis. **b.** Csp^3-Csp^2 cross coupling of organoboranes is typically achieved under aqueous basic conditions. 1,2-Metallate reactions of boronic esters achieve Csp^3-Csp^3 bond formation by using Grignard and organolithium reagents. **c.** Conditions permissive of Csp^3-C bond formation cleave MIDA boronates and are therefore incompatible with automated lego-like synthesis. TIBO = 2,4,6-triisopropylbenzoate.

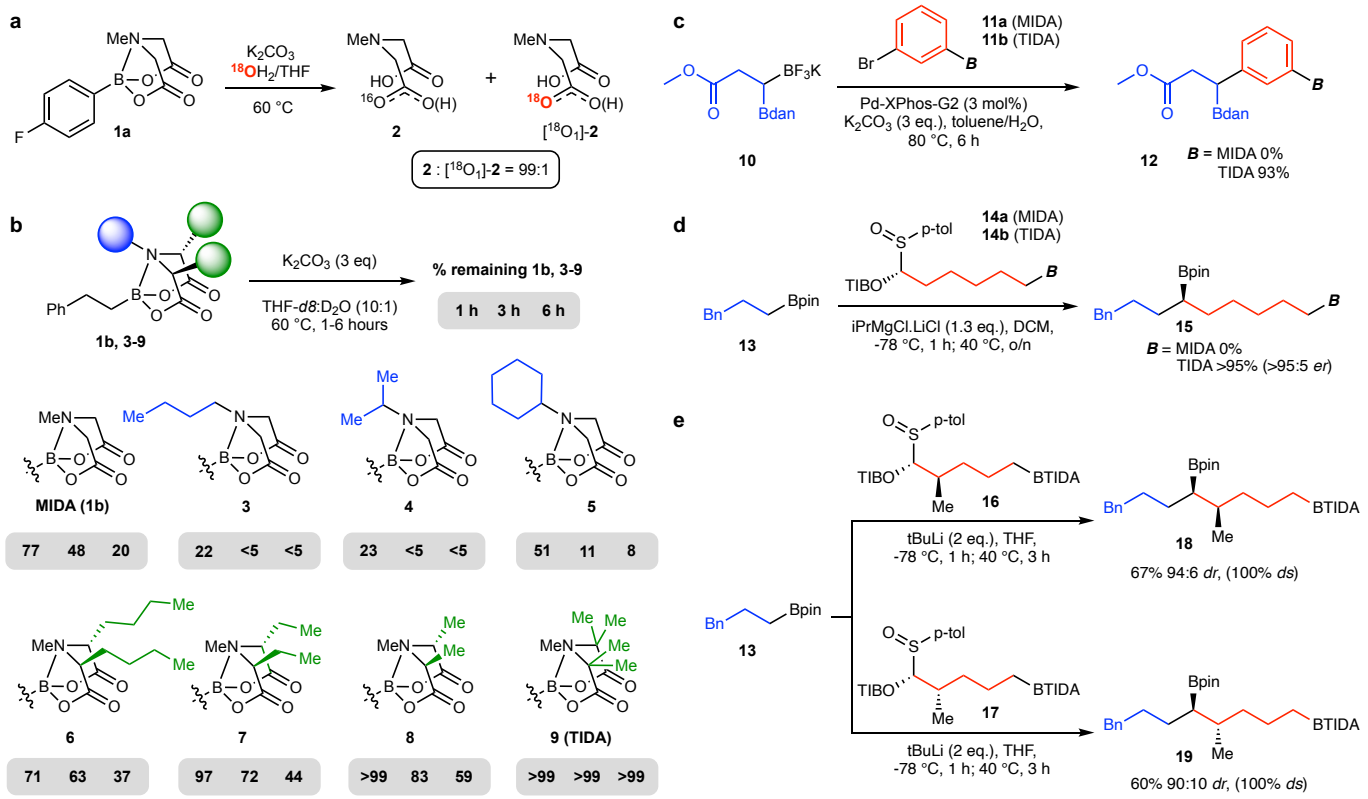

Fig. 2 | TIDA boronates are exceptionally stable toward hydrolytic and nucleophilic cleavage. a. MIDA boronate **1a** is hydrolyzed *via* N–B bond-mediated water activation under standard stereospecific Csp^3 coupling conditions. **b.** Modifications of the MIDA ligand yield varying degrees of stability for the corresponding iminodiacetic acid boronates under common aqueous basic stereospecific Csp^3-Csp^2 coupling conditions. TIDA boronate **9** is exceptionally stable. **c.** TIDA boronates resist hydrolysis during Csp^3-Csp^2 Suzuki-Miyaura coupling with **10** whereas MIDA boronates are completely hydrolyzed. **d.** TIDA boronates were stable to the Grignard reagent iPrMgCl.LiCl to allow Csp^3-Csp^3 bond forming 1,2-metallate reactions, whereas MIDA boronates were cleaved under these conditions. **e.** TIDA boronates remarkable stability extends to tBuLi. Diastereospecificity (*ds*) = (final diastereoisomeric ratio/initial diastereoisomeric ratio) x 100. Enantiomeric ratio (*er*).

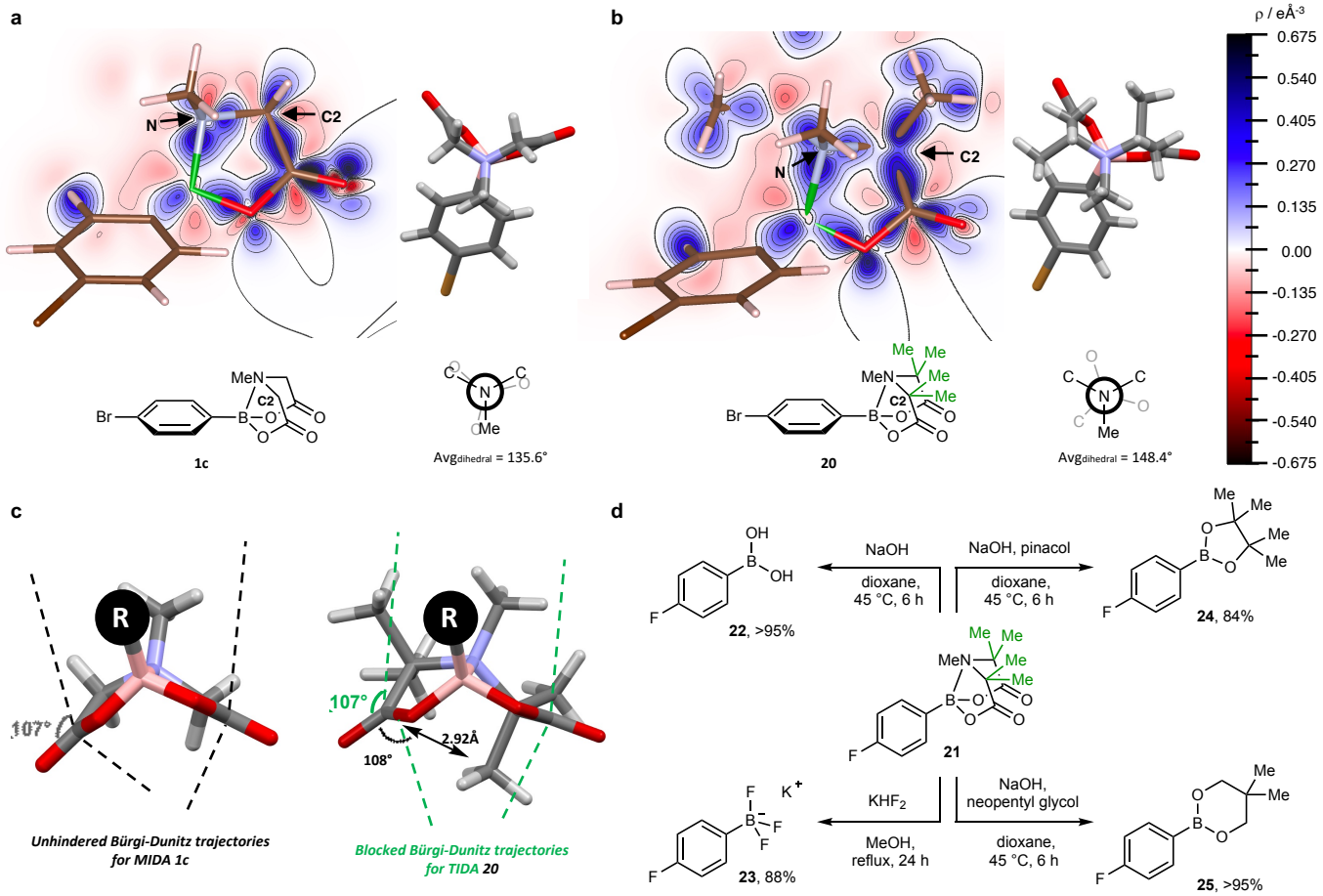

Fig. 3 | Steric and electronic effects collaborate to stabilize TIDA boronates. a. Examination of non-spherical (i.e. bonding) electron density (ρ) in the plane of iminodiacetic acid ring of MIDA boronate **1c**. Contour level 0.0675 eA^{-3}. Shown inset is the perspective looking down from N to B. **b.** Non-spherical electron density in the plane of iminodiacetic acid ring of TIDA boronate **12** shows substantial electronic redistribution compared to MIDA boronate **1c**, particularly for the N-B bond. An associated 12° torsional shift increased hyperconjugative interactions along the N-B axis compared to MIDA **1c**. **c.** Comprehensive steric shielding of all 4 π-faces of TIDA boronates suppresses nucleophilic attack on the carbonyl carbons. **d.** Despite their high stability toward Csp^3 bond forming reactions TIDA boronates are easily removed under aqueous or protic conditions at elevated temperatures. Contour plots were generated using VESTA 3[51].

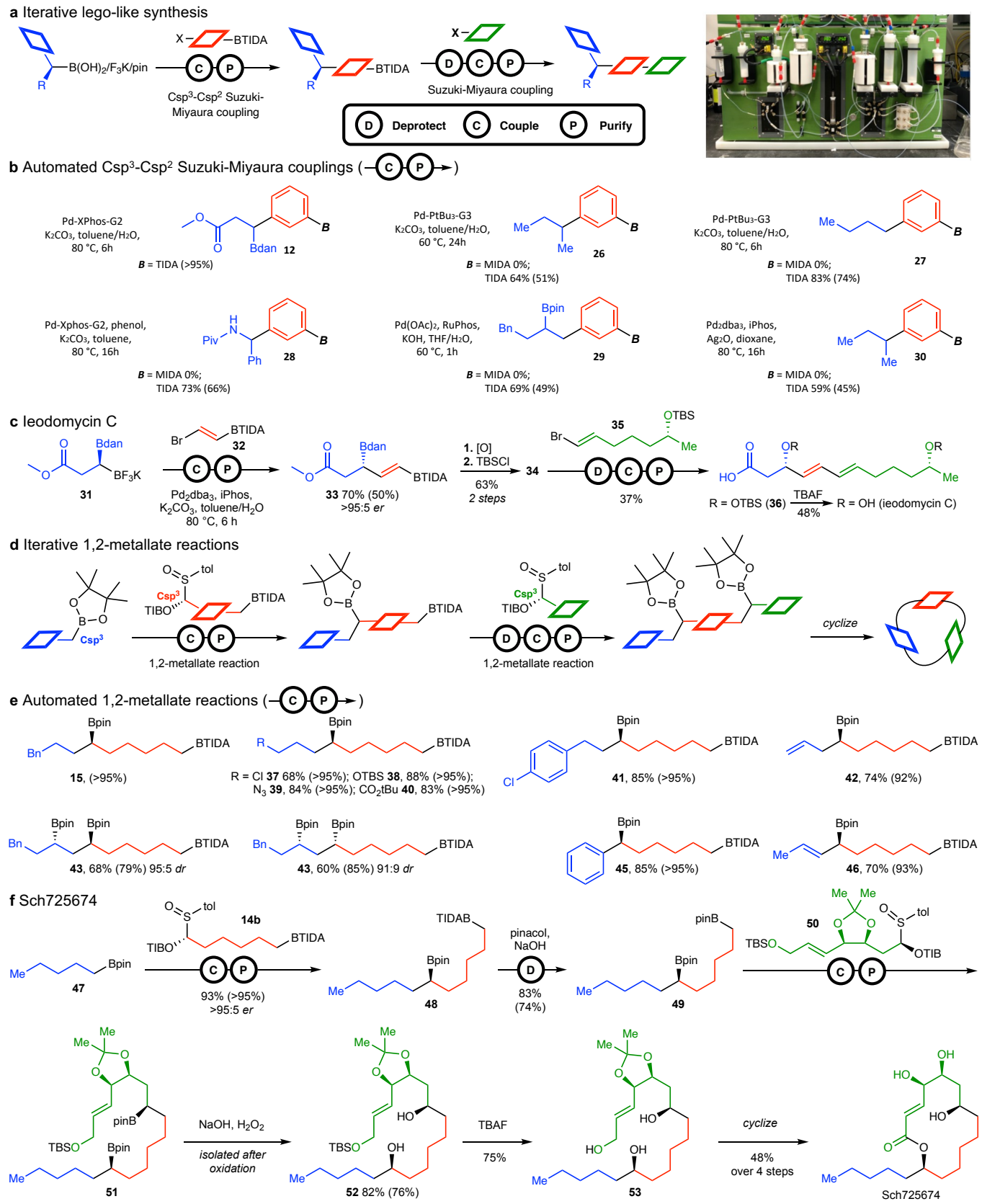

Fig. 4 | TIDA boronates enable automated assembly of Csp³ boronate building blocks. a. TIDA boronates enable iterative Suzuki-Miyaura cross-coupling. **b.** Assembly of Csp^3 building blocks *via* Csp^3-Csp^2 Suzuki-Miyaura cross-coupling enabled by TIDA boronates. MIDA boronates universally provided no product. **c.** Automated stereospecific Csp^3 cross coupling with TIDA boronate **34** enables lego-like synthesis of ieodomycin C. **d.** TIDA boronates enable iterative 1,2-metallate reactions. **e.** Assembly of Csp^3 building blocks *via* Csp^3-Csp^3

bond forming 1,2-metallate reactions enabled by TIDA boronates. **f.** Sequential automated stereospecific Csp^3-Csp^3 bond formation enabled by TIDA boronates allows lego-like synthesis of sch725674. For detailed experimental procedures see supplementary information. Yields for automated synthesis shown in parentheses. Enantiomeric ratio (*er*). Diastereoisomeric ratio (*dr*).

Data Availability: X-ray crystal structure data are available free of charge on the Cambridge Crystallographic Data Centre under the following accession numbers :- 4-bromophenyl MIDA boronate **1c**: *structure* 2087874, *multipole refinement* 2087875; 4-bromophenyl TIDA boronate **20**: *structure* 2087872, *multipole refinement* 2087873; 3-bromophenyl dimethyl MIDA boronate **SI-10**: *structure* 2087648; ethynyl TIDA boronate **SI-47**: *structure* 2087715; *cis*-2-bromovinyl TIDA boronate **SI-49**: *structure* 2087714; *trans*-2-bromovinyl TIDA boronate **32**: *structure* 2087712; sulfinyl benzoate *anti*-**SI-25** *structure* 2087716; TIDA anhydride *structure* 2120500. All other data are available in the main text or the supplementary materials.

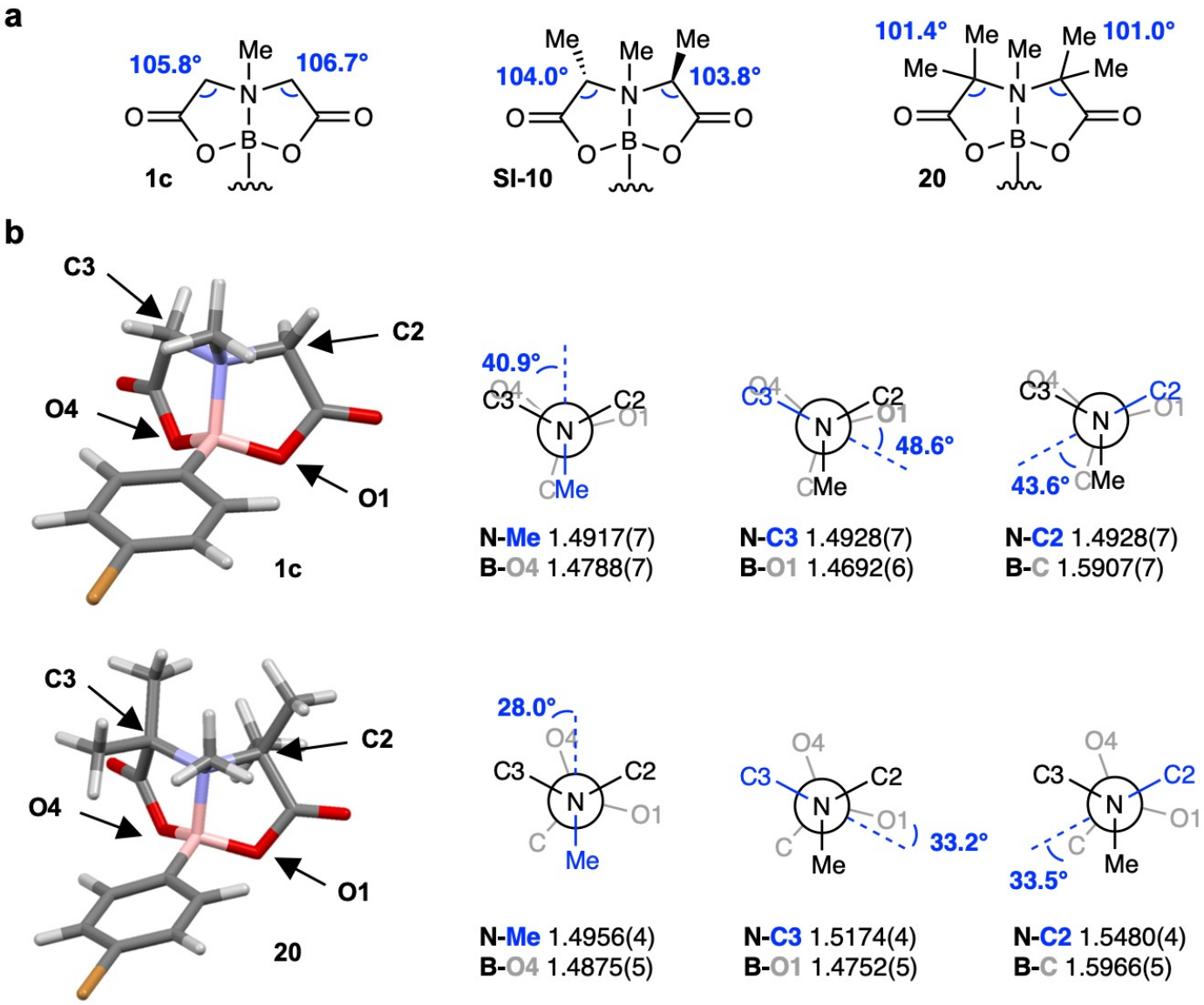

Extended Data Figure 1 | Structural consequences of backbone substitution on iminodiacetic acid boronates. a. Internal angle compression from MIDA **1c** to dimethyl MIDA **SI-10** to TIDA **20** suggest thermodynamic Thorpe-Ingold effects might further support hyperconjugative interactions by rigidifying the iminodiacetic acid cage of TIDA. **b.** Increases in nitrogen attached donor and boron attached acceptor bond lengths for TIDA **20** compared to MIDA **1c** support hyperconjugative transfer of electron density along the N-B bond (lengths in Å).

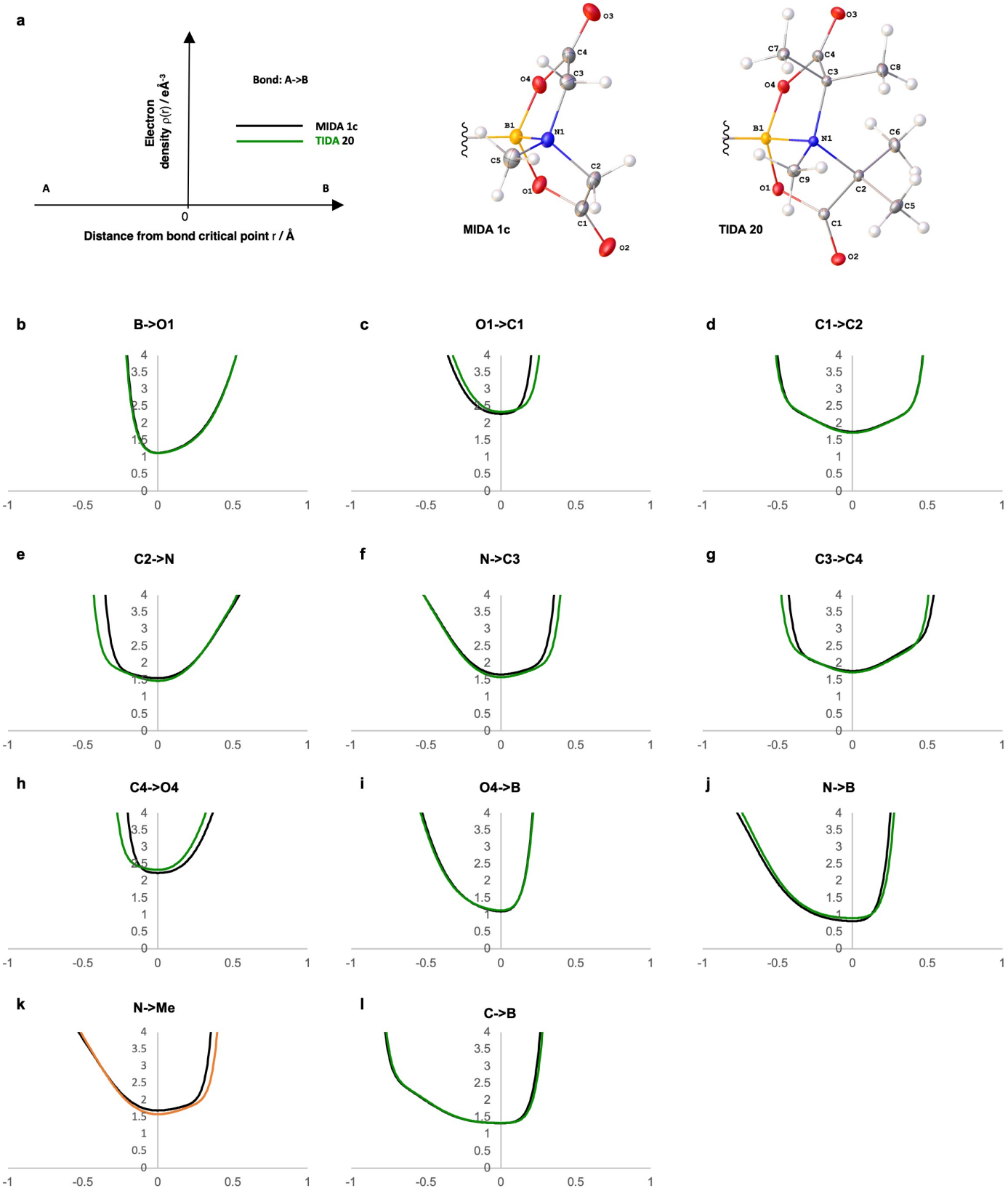

Extended Data Figure 2 | Bond path total electron density for MIDA boronate 1c and TIDA boronate 20 a Legend and numbered molecular structures. Sections **b** through **i** follow anticlockwise around the iminodiacetic acid cage. The N-B, N-Me, and C-B bonds are also included (**j-l**). The maximum displayed value of the electron density (y-axis) is capped at 4 eA^{-3} to best capture the interatomic bonding region.

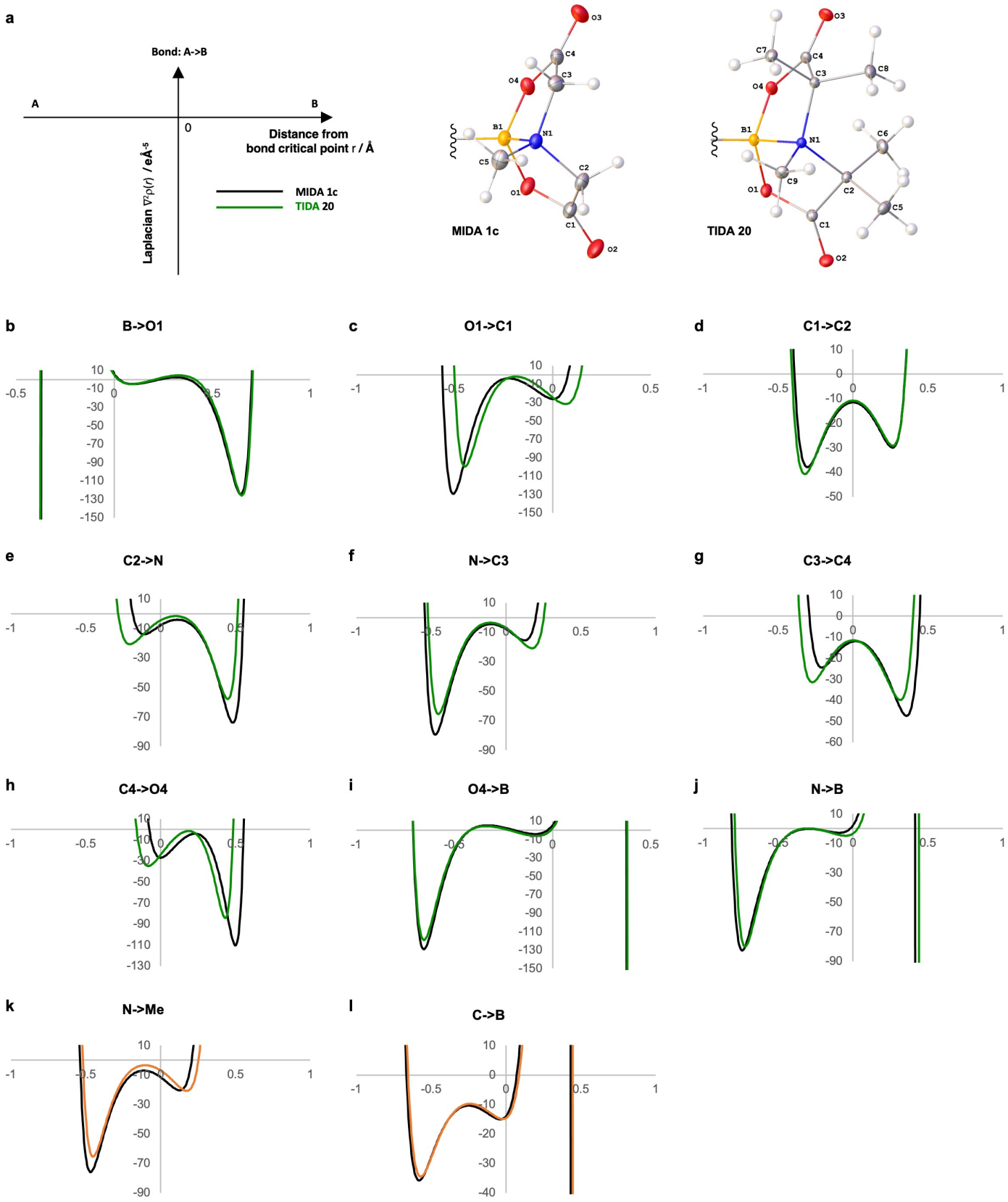

Extended Data Figure 3 | Bond path Laplacian profiles comparing MIDA boronate 1c and TIDA boronate 20. **a** Legend and labelled structures. **b** through **i** follows an anticlockwise path around MIDA **1c** and TIDA **20** as well as the N-B, N-Me, and C-B bonds (**j-l**).

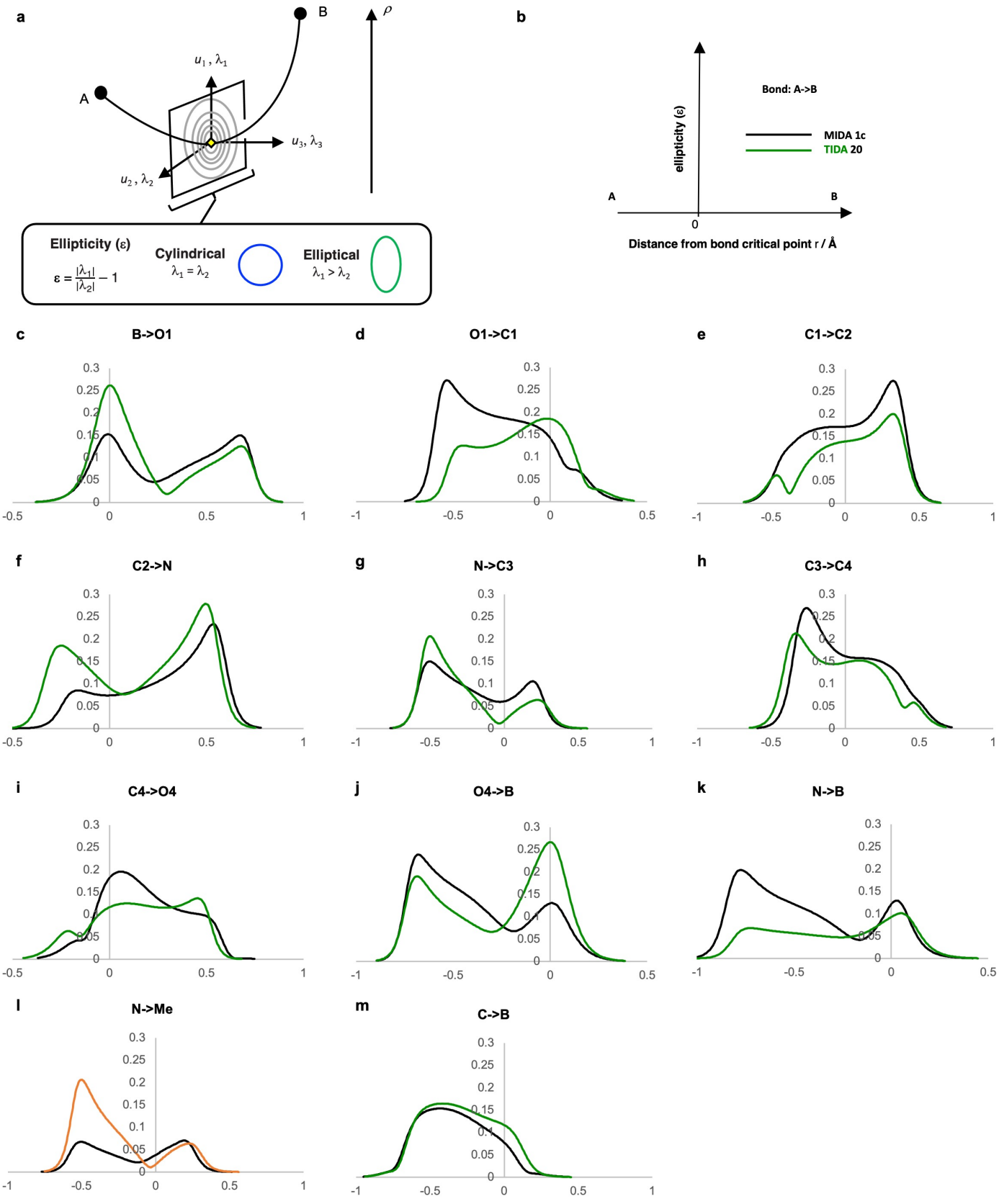

Extended Data Figure 4 | Bond path ellipticity profiles for MIDA boronate 1c and TIDA boronate 20 a Schematic representation of ellipticity, which reflects an increase in directionality of electron density and is characteristic of increased π-character. **b** Legend for sections **c** to **m**. Pronounced changes in ellipticity can be seen for TIDA boronate **20** compared to MIDA boronate **1c** particularly for the N-C2/3 (**f**,**g**), B-O1/4 (**c**, **j**), and N-B bonds, which are consistent with observations of redistributions of electron density around the N-B bond (see Fig 3c and 3d). Ellipticity profiles (**c** to **j**) follow an anticlockwise path around the iminodiacetic acid rings

of **1c** and **20** starting with B-O1 (**c**) and ending with O4-B (**j**). Profiles for the N-B, N-Me, and C-B bonds (**k**-**m**) are also included.

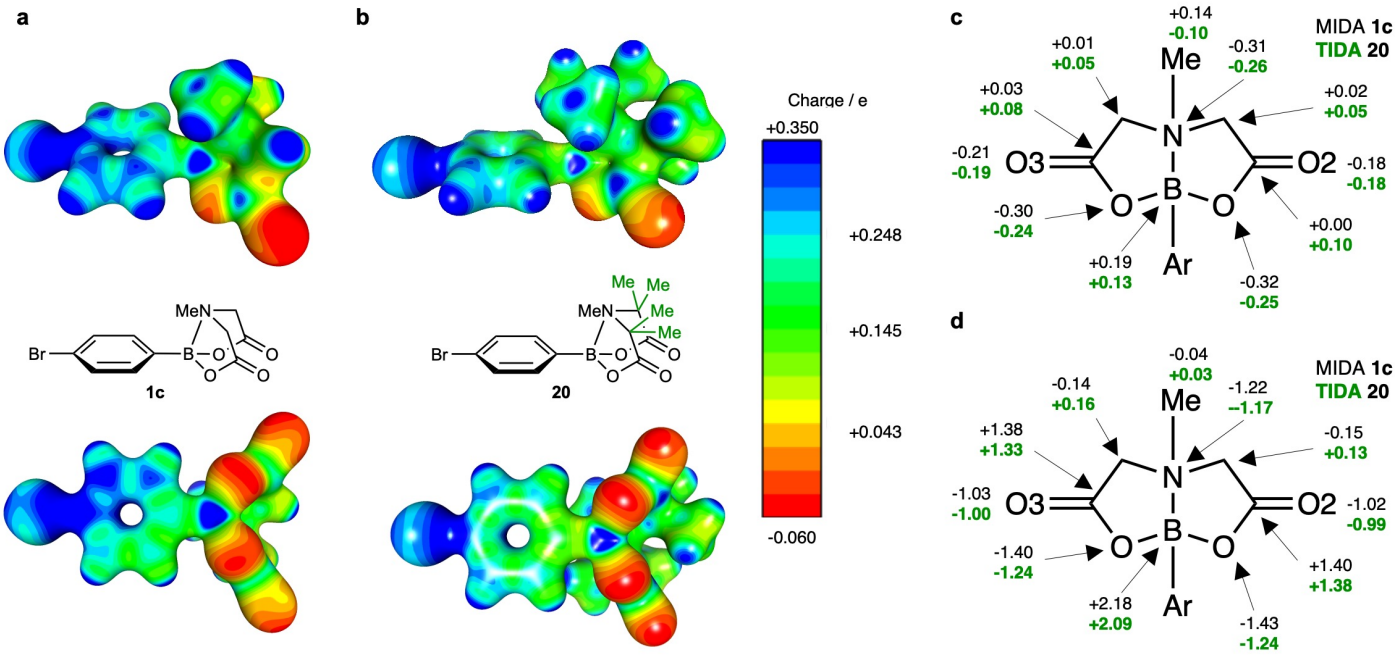

e

	δ_C (C=O) acetone-d_6		δ_B acetone-d_6	
	MIDA	TIDA	MIDA	TIDA
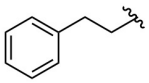	168.9[a]	175.1	12.9[a]	10.5
	169.0[b]	175.1	12.8	10.6
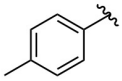	169.3[c]	175.7	11.8[c]	9.3
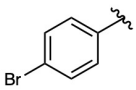	169.2[c]	175.3	11.4[c]	9.3

[a]*Eur. J. Inorg. Chem.* **2020**, 1995; [b]*Tetrahedron* **2009**, *65*, 3130; [c]*Chem. Eur. J.* **2020**, *26*, 3738

f

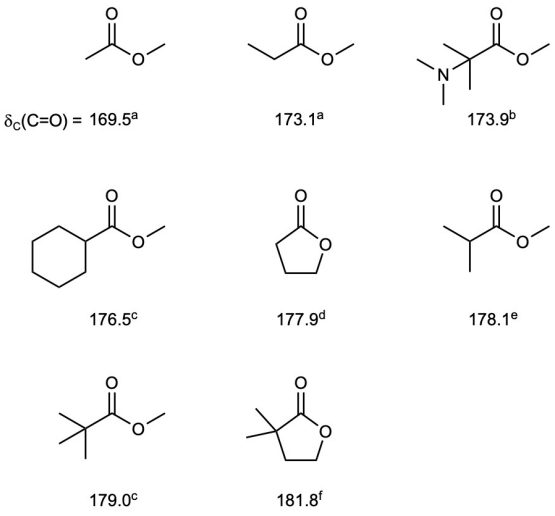

[a]*JOC* **2002**, *67*, 6995; [b]*ACIE* **2012**, *51*, 10808; [c]*JACS* **2019**, *141*, 11161; [d]*JACS* **2015**, *137*, 3767; [e]*JACS* **1990**, *112*, 8598; [f]*Chem. Eur. J.* **2011**, *17*, 8555

Extended Data Figure 5 | Charge analysis of MIDA boronate 1c and TIDA boronate 20. a Electrostatic potential surface for MIDA **1c**, showing side on and bottom perspectives. **b** Electrostatic potential surface for TIDA **20**, showing side on and bottom perspectives. **c** Stockholder charges comparing MIDA **1c** (black) and TIDA **20** (green), values shown are in electrons. **d** Integrated charge comparing MIDA **1c** (black) and TIDA **20** (green), values shown are in electrons. TIDA backbone methyl groups were omitted for clarity on the charge plots. **e** A downfield shift for TIDA boronates carbonyl carbons indicates a net electron depletion relative to MIDA boronates. Similarly, there is an upfield shift for the boron atoms in TIDA boronates relative to MIDA boronates indicating increased boronate complex-like character and elevated electronic shielding. **f** Trends in ^{13}C NMR carbonyl chemical shifts in $CDCl_3$ upon sequential substitution of the α-carbon with methyl groups and/or lactone formation and/or addition of an α-dimethylamino group are provided for comparison.

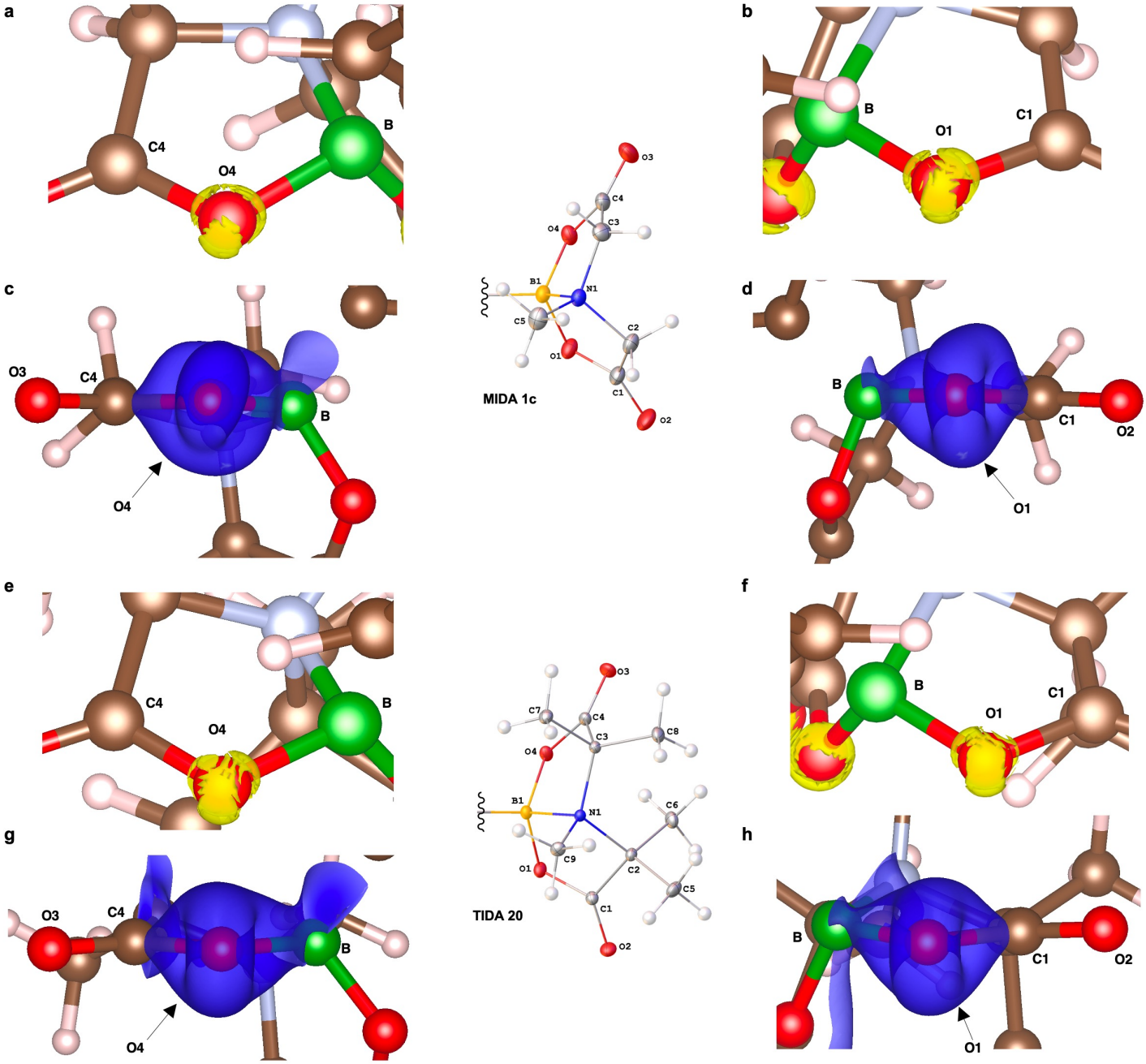

Extended Data Figure 6 | Laplacian and electron density isosurfaces support redistributed density around the O4-B-O1 linkage of TIDA 20 a The Laplacian at isosurface value -80 eA^{-5} (shown in yellow) for MIDA **1c** indicates an isolated valence shell charge concentration (VSCC) at O4 (i.e. minimal lone pair interactions). **b** Unlike at O4 the Laplacian at O1 for MIDA **1c** reveals coalescence of lone pair VSCC and the O1-C1 VSCC, pointing toward interaction between O1 and C1 (the adjacent carbonyl). **c** End-on view of deformation density (isosurface value of 0.0034 eA^{-3} in blue) down O4 in MIDA **1c** provides further evidence for charge localization at O4. **d** In contrast to O4 the end-on view of deformation density down O1 for MIDA **1c** reveals the electron distribution along B-O1-C1, favors O1-C1. **e** The Laplacian of TIDA **20** reveals interaction between lone-pair VSCC and both C4-O4/O4-B VSCCs. **f** In contrast to MIDA **1c** the lone pair VSCC of TIDA **20** at O1 coalesces with the B-O1 VSCC and not the O1-C1 VSCC. Consistent with these changes in VSCCs, deformation density at O4 (**g**) and O1 (**h**) for TIDA **20** supports electronic redistribution about the C4-O4-B-O1-C1 network compared to MIDA **1c**.

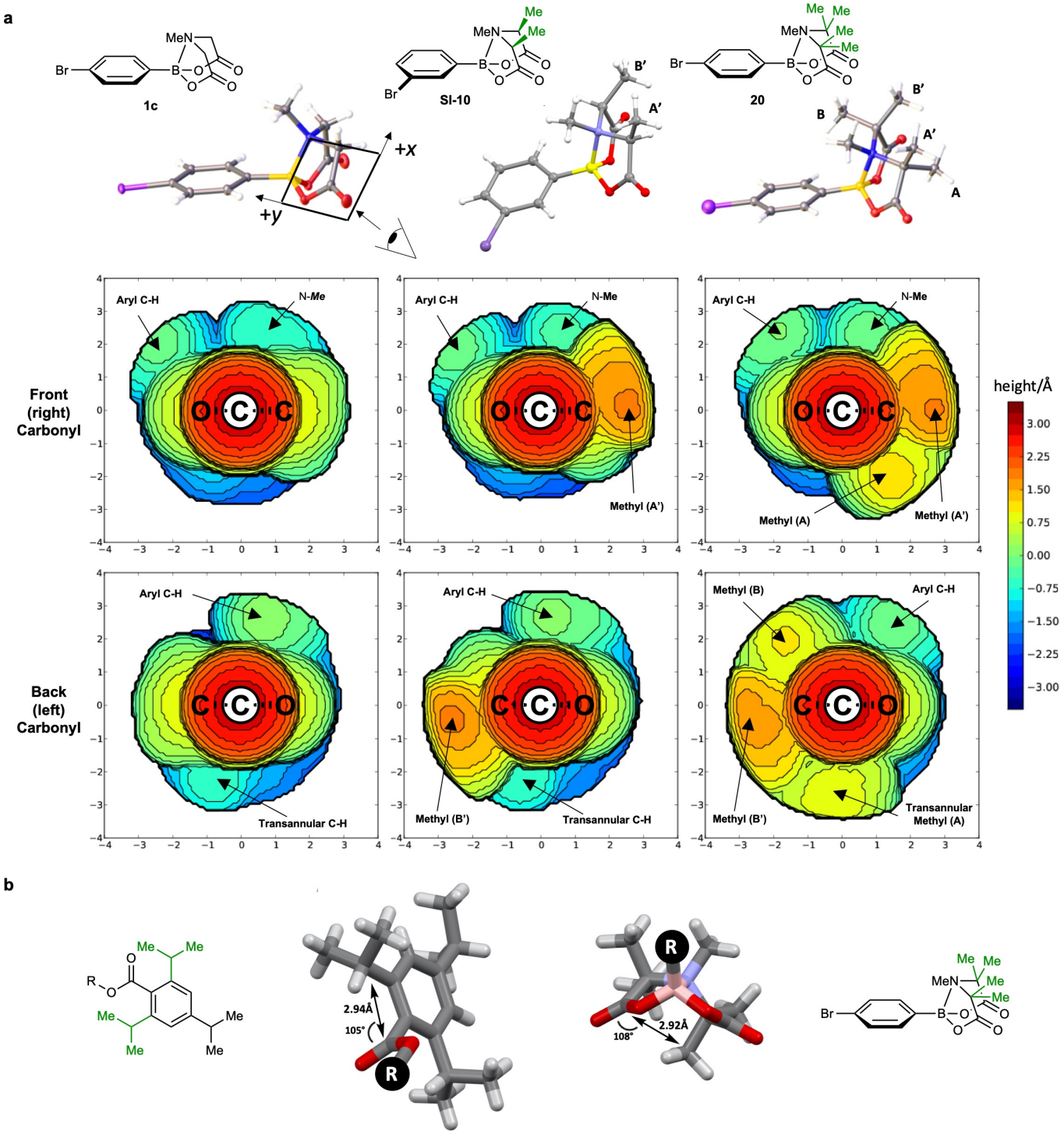

Extended Data Figure 7 | Robust steric shielding suppresses carbonyl attack on TIDA boronates a. Topological steric maps[43] of the plane perpendicular to the carbonyl carbons enable comparison of MIDA (**1c**), dimethyl-MIDA (**SI-10**), and TIDA (**20**). MIDA boronates (left column) experience minimal steric shielding, and methyl groups introduced in dimethyl-MIDA (A' and B') occupy pseudo-equatorial positions, minimally impacting carbonyl approach (center column). The two additional methyl groups in TIDA (A and B) occupy pseudo axial positions and establish transannular steric shielding interactions between A and the carbonyl on the opposite side of the TIDA framework (right column). Additionally, A and B shield their adjacent carbonyls towards approach at the Burgi-Dunitz angle**. b.** The transannular influence of A mirrors that of Beak-type 2,4-6-triisopropyl benzoates which are resistant to carbon centered nucleophiles.

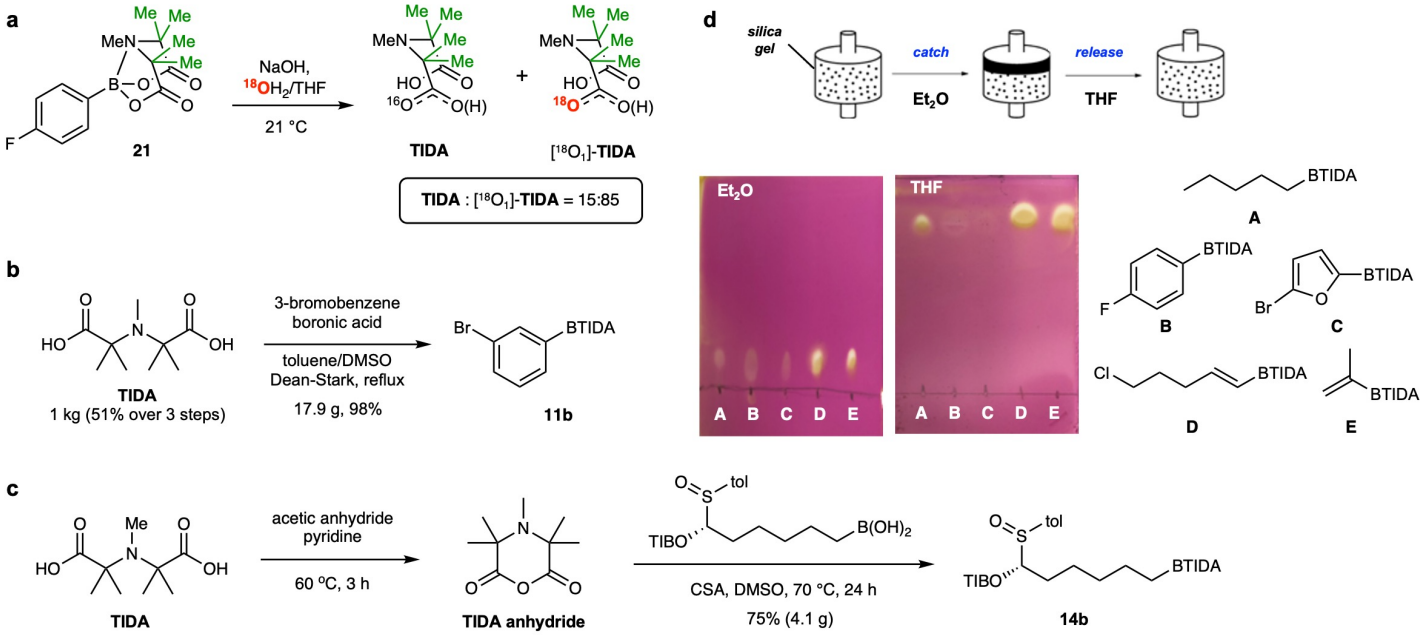

Extended Data Figure 8 | TIDA boronates retain all required properties to enable generalized automated synthesis. a. TIDA boronate **21** is hydrolyzed by NaOH primarily *via* the ester hydrolysis mechanism. **b.** TIDA ligand and TIDA boronates can be prepared on scale. **c.** TIDA anhydride provides an alternative method to prepare TIDA boronates. **d.** TIDA boronates possess a binary affinity for silica gel, agnostic of the attached carbon fragment. They are minimally mobilized in Et_2O and rapidly eluted in THF, enabling generalized and automatable catch-and-release purification.

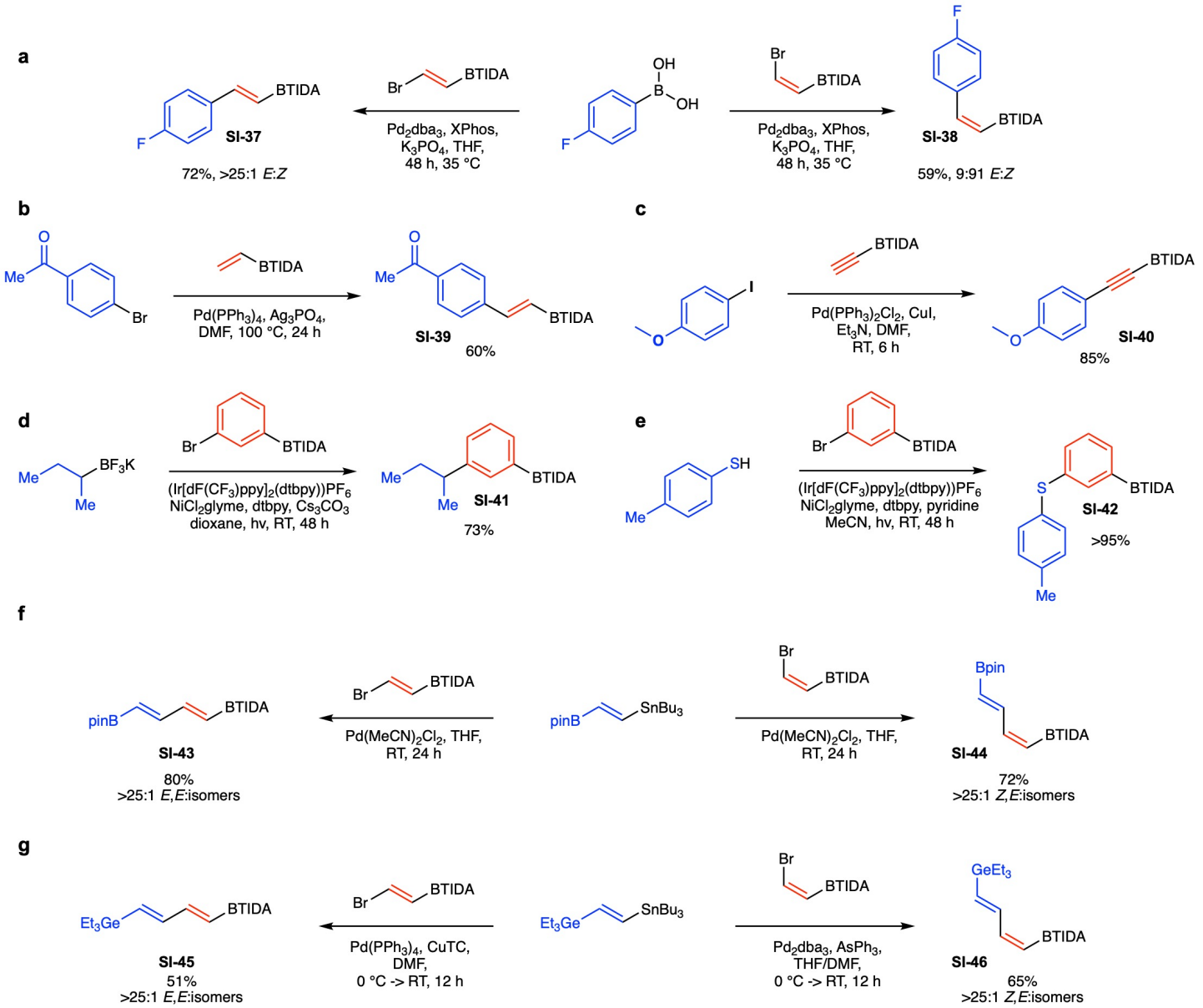

Extended Data Figure 9 | TIDA boronates tolerate a diverse range of cross coupling chemistry a. Suzuki-Miyaura cross coupling. **b.** Heck coupling. **c.** Sonogashira coupling. **d.** Photochemical Suzuki-Miyaura cross coupling. **e.** Photochemical thioetherification. **f.** Stille coupling leading to bis-borylated dienes. **g.** Stille coupling leading to germylated dienes.

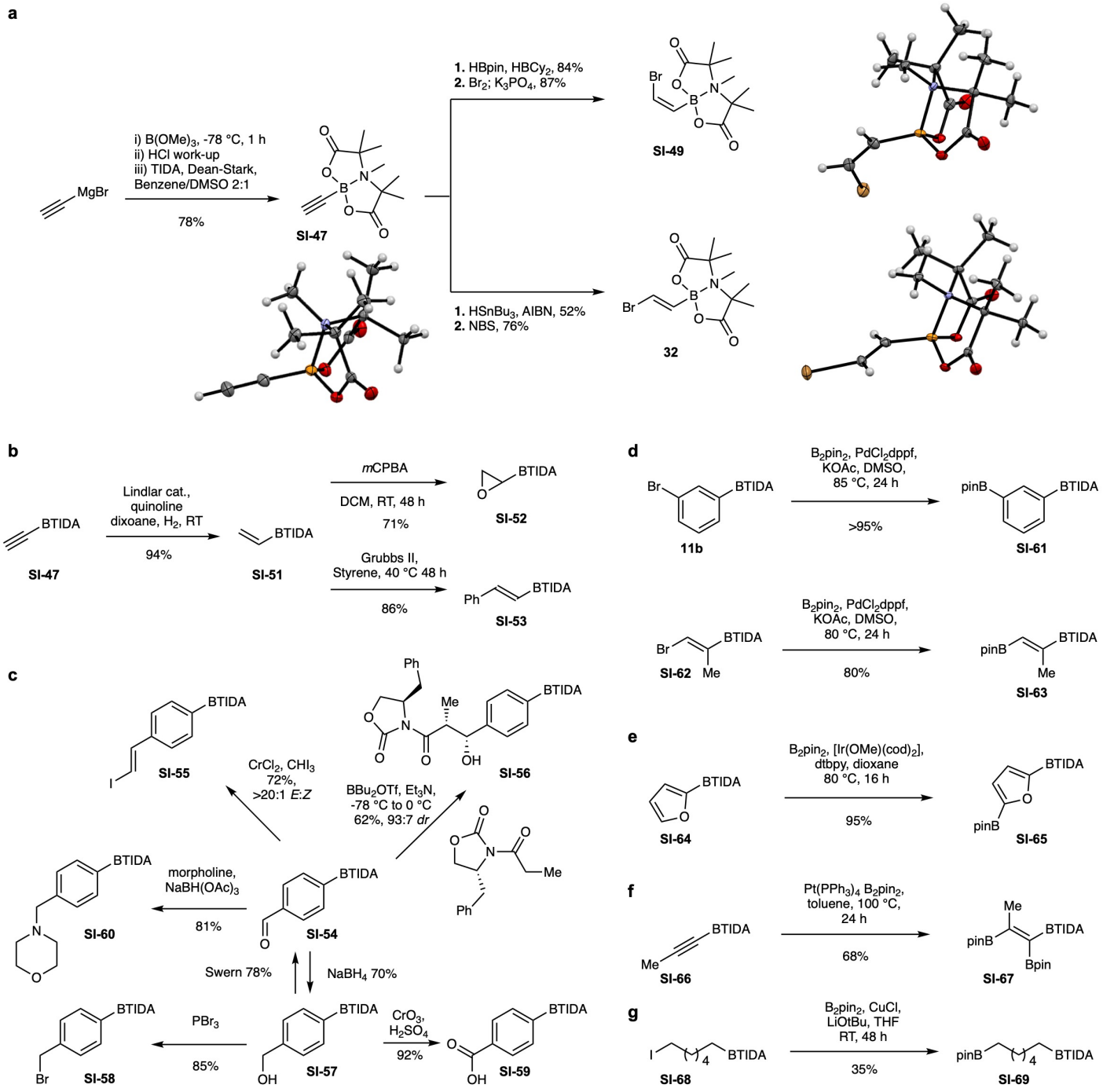

Extended Data Figure 10 | Functional group interconversion of TIDA boronate building blocks. a. Ethynyl TIDA boronate is readily converted into *E*- and *Z*- 2-bromovinyl TIDA boronate with excellent stereocontrol. Images of X-ray crystal structures shown inset. **b.** Reduction of ethynylTIDA boronate furnishes vinyl TIDA boronate which participates in epoxidation and Grubbs metathesis. **c.** Common functional group interconversion reactions are well tolerated by TIDA including oxidation, reduction, halogenation, reductive amination, Evans aldol, and Takai olefination. A wide range of borylation chemistries are tolerated by TIDA boronates to produce mono-protected polyborylated building blocks, including Miyaura (**d**), C-H borylation (**e**), diboration (**f**), and copper catalyzed borylation (**g**).